

PAPER • OPEN ACCESS

Control of temperature dependent viscosity for manufacturing of Bi-doped active fiber



To cite this article: Rui Duan *et al* 2024 *Int. J. Extrem. Manuf.* **6** 035504

View the [article online](#) for updates and enhancements.

You may also like

- [Water/DMSO-Based Hybrid Electrolyte and Urea Additive Engineering for Performance Regulation in Aqueous Sodium Batteries](#)
xiang Zhou, Hailin Shen, Xiaohui Chen et al.
- [Drift suppression of solution-gated graphene field-effect transistors through electrolyte submersion](#)
Shota Ushiba, Yuka Tokuda, Tomomi Nakano et al.
- [Improving fatigue properties of normal direction ultrasonic vibration assisted face grinding Inconel 718 by regulating machined surface integrity](#)
Nianwei Xu, Renke Kang, Bi Zhang et al.

Control of temperature dependent viscosity for manufacturing of Bi-doped active fiber

Rui Duan^{1,2}, Jingfei Chen^{1,2}, Hao Ke^{1,2}, Tianxia Wei^{1,2}, Ke Zhang^{1,2}, Xueliang Li^{1,2}, Xu Feng^{1,2,*}, Qiuju Zheng³, Zhixue He⁴, Jianrong Qiu⁵  and Shifeng Zhou^{1,2,4,*} 

¹ State Key Laboratory of Luminescent Materials and Devices, School of Materials Science and Engineering, South China University of Technology, Guangzhou 510640, People's Republic of China

² Guangdong Provincial Key Laboratory of Fiber Laser Materials and Applied Techniques, Guangdong Engineering Technology Research and Development Center of Special Optical Fiber Materials and Devices, Guangzhou 510640, People's Republic of China

³ School of Materials Science and Engineering, Qilu University of Technology, Jinan, People's Republic of China

⁴ Peng Cheng Laboratory, Shenzhen 518000, People's Republic of China

⁵ College of Optical Science and Engineering, State Key Laboratory of Modern Optical Instrumentation, Zhejiang University, Hangzhou 310027, People's Republic of China

E-mail: msfx@mail.scut.edu.cn and zhoushifeng@scut.edu.cn

Received 25 July 2023, revised 14 January 2024

Accepted for publication 12 March 2024

Published 2 April 2024



CrossMark

Abstract

Bi-activated photonic materials are promising for various applications in high-capacity telecommunication, tunable laser, and advanced bioimaging and sensing. Although various Bi-doped material candidates have been explored, manufacturing of Bi heavily doped fiber with excellent optical activity remains a long-standing challenge. Herein, a novel viscosity evolutional behavior mediated strategy for manufacturing of Bi-doped active fiber with high dopant solubility is proposed. The intrinsic relation among the evolution of Bi, reaction temperature and viscosity of the glass system is established. Importantly, the effective avenue to prevent the undesired deactivation of Bi during fiber drawing by tuning the temperature dependent viscosity evolution is built. By applying the strategy, for the first time we demonstrate the success in fabrication of heavily doped Bi active fiber. Furthermore, the principal fiber amplifier device is constructed and broadband optical signal amplification is realized. Our findings indicate the effectiveness of the proposed temperature dependent viscosity mediated strategy for developing novel photonic active fiber, and they also demonstrate the great potential for application in the next-generation high-capacity telecommunication system.

Supplementary material for this article is available [online](#)

Keywords: infrared luminescence, active fiber, optical amplification

* Authors to whom any correspondence should be addressed.



Original content from this work may be used under the terms of the [Creative Commons Attribution 4.0 licence](#). Any further distribution of this work must maintain attribution to the author(s) and the title of the work, journal citation and DOI.

1. Introduction

The transmission capacity crunch of optical communication systems has become a prominent bottleneck issue in the era of big data [1, 2]. Currently, multi-band transmission technology, based on the exploitation of new optical wavelength bands including L-, S-, E- and O-band, is widely recognized as one of the effective approaches to extend the transmission capacity [3–5]. In this technology, a broadband fiber amplifier which can work in various communication wavelength bands is the key device and has been actively explored. Especially, Bi-activated gain materials and fiber amplifiers have drawn much attention due to the interesting broadband near-infrared (NIR) optical response that covers nearly all telecommunications windows in the range from 1100 nm to 1700 nm [6, 7]. Importantly, many Bismuth (Bi)-doped fiber amplifiers working in O, E, L and U bands have been developed over the past decades [8]. For example, the first Bi-doped glass fiber was fabricated and found to show optical amplification at a wavelength of 1300 nm [9]. Later, Bi-doped phosphosilicate and germanosilicate glasses and fibers were invented and demonstrated to provide efficient optical amplification in a wide wavelength range of 1270 ~ 1800 nm [10–14]. Importantly, the principal fiber amplifier device was also developed by the company of optical fiber cable and connectivity solutions [15–17].

Despite of above substantial progress, there are still some long-standing challenges for the future development and wide commercial applications of Bi-active fiber and device. Firstly, the solubility of Bi in the above glass matrix is relatively low (up to 0.02 at%) [18] and rather long active fiber (up to tens of meters) [9] is necessary to achieve high gain. A novel glass system with high Bi solution is expected. Secondly, to the best of our knowledge, the existing Bi-doped fibers with net gain effect for optical amplification and even laser can only be fabricated by a few groups in the world, which are fabricated by unique chemical vapor deposition (CVD) methods and the most key process is even confidential. The complicated CVD technique not only constructs a huge technique barrier for the fabrication of Bi-active fiber but also limits the available glass fiber system. And thus, much simpler fiber fabrication technique such as rod-in-tube is strongly demanded [19–21].

To overcome this limitation, the strategy to increase Bi concentration by using multicomponent bulk glass systems was proposed and the concentration can reach 0.2 mol% in silicate glass, 1.0 mol% in germanate glass and 1.0 mol% in phosphate glass. Unfortunately, fabrication of them into activated fiber via rod-in-tube technique has been met with limited success because of the unexpected Bi de-activation during high-temperature fiber drawing process. Therefore, it is critical to explore a novel strategy to maintain the activity during fiber fabrication for the glass systems with high Bi solubility.

Here, we propose a viscosity evolutionary behavior mediated strategy for manufacturing of Bi-doped active fiber with high dopant solubility. The viscosity evolution behavior during cooling is classified between ‘strong’ and ‘fragile’, which can

be evaluated by the melt fragility index parameter m [22–28]. We build a relationship among the evolution of Bi, reaction temperature and viscosity as well as the melt fragility index parameter m of the glass system. Importantly, it is found that tuning the temperature dependent viscosity variation curve can help to avoid the unexpected overlapping between Bi activation during melting and deactivation during fiber drawing. Following the above rule, for the first time we demonstrate the success in fabrication of heavily doped Bi active fiber (3 mol%) by rod-in-tube method. Furthermore, the principal fiber amplifier device is constructed and broadband optical amplification is realized. The results indicate that the proposed viscosity evolutionary behavior mediated strategy provides a new opportunity for development of active fiber device with high compactness.

2. Results and discussion

2.1. Control of temperature dependent viscosity strategy for manufacturing of Bi-doped active fiber

In contrast to the conventional active dopants such as rare earth and transition metal ions which have fixed valence state, Bi belongs to the main group ions and is featured by the existence of rich configurations. Recently, various Bi centers (e.g. Bi^{5+} , Bi^{3+} , Bi^{2+} , Bi^+ , Bi^0 , Bi clusters and even nanocrystals) have been identified, and the usual metastable centers such as Bi^+ , Bi^0 and Bi clusters are regarded as the Bi active centers (BACs) which contribute to the NIR activity [14, 26]. During the manufacturing of Bi-doped active fiber, these centers experienced the complicate and thermodynamic chain reactions of Bi metal particles $\leftrightarrow \text{Bi}^{3+} \leftrightarrow \text{Bi}^+/\text{Bi}^0 \leftrightarrow \text{Bi}$ clusters and distinct centers are stabilized at various states [27].

The manufacturing of Bi-doped active fiber contains two processes: the fabrication of Bi-activated bulk precursor glass rod and rod-in-tube fiber drawing. The Bi-activated bulk precursor glass rod is fabricated by the melt-quenching method, operating at the temperature higher than the melting point (T_M). Figure 1(a) summarize the corresponding evolution of Bi centers during melting. The chain reaction goes forward as the temperature increases, leading to the formation of thermostable BACs at high temperature. Appropriate high temperature and fast quenching process facilitate the acquisition of maximum concentration of BACs on the premise of less Bi volatilization at even room temperature for the preparation of the Bi-activated bulk precursor glass rod.

In contrast, rod-in-tube fiber drawing process is operated at temperature between glass transition temperature (T_g) and T_M , where the glass rod would re-heated to nonequilibrium supercooled liquid state. As shown in figure 1(b), in such supercooled liquid state, BACs are energetically metastable and they exhibit great tendency toward Bi metal particles, resulting in the serious degradation and even loss of the activity. Unluckily, for almost all of the reported system, this deactivation stage presents strong overlapping with the conventional rod-in-tube fiber drawing operation window.

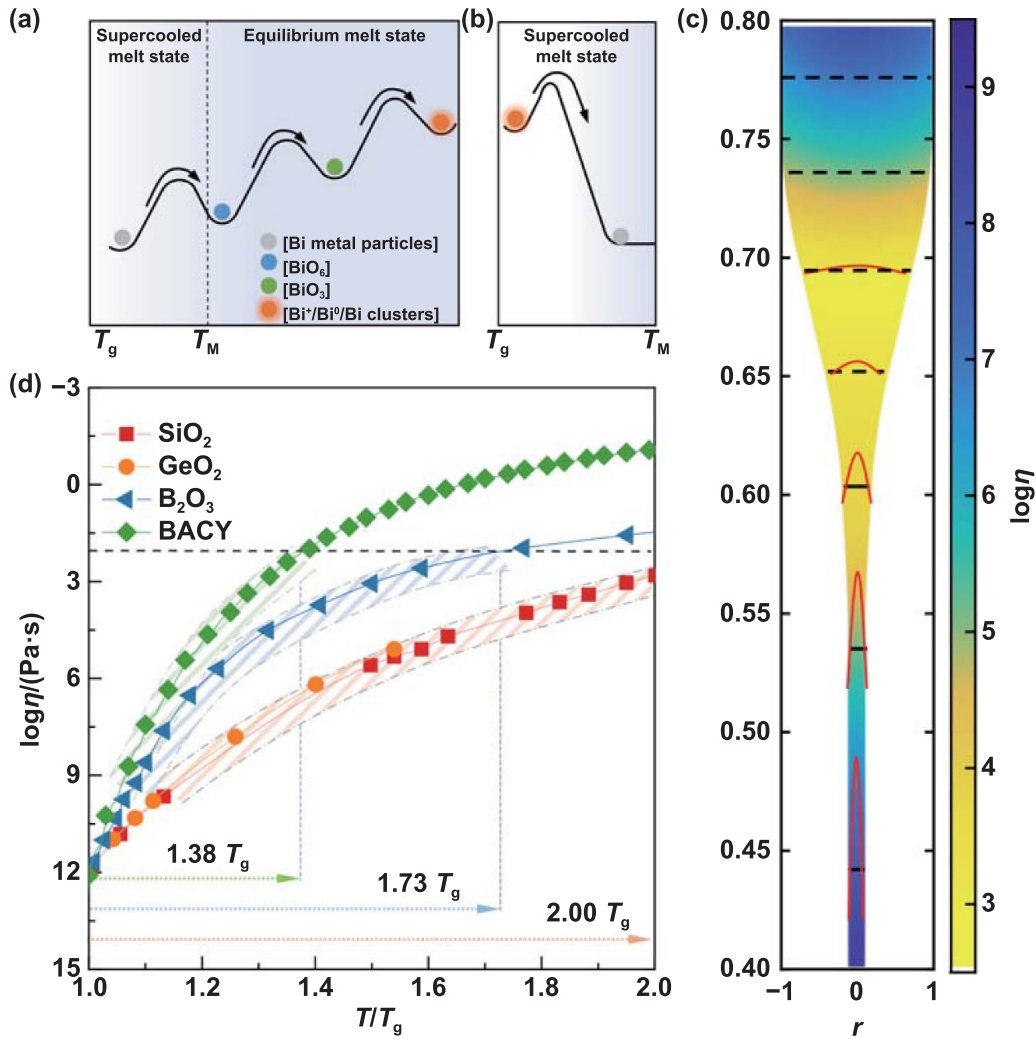


Figure 1. Illustration of the proposed viscosity evolutionary behavior mediated strategy. (a), (b) Schematic illustration of the forming energy barrier of Bi active centers (a) in the melt state and (b) supercooled liquid state. (c) The calculated radial distribution of viscosity during the thermal drawing process (Reproduced from [28], CC BY 4.0.). (d) Pattern of viscosity-temperature relations for T_g -based normalization (the slash section indicates as the classical fiber-drawing required viscosity region). Using SiO₂ and GeO₂ as the typical examples of low melt fragility, and B₂O₃ and BACY as the examples of high melt fragility.

Keeping above key issues in mind, we devote our efforts to prevent the unexpected Bi deactivation during fiber drawing. From the viewpoint of kinetics, based on Arrhenius law, the deactivation of Bi centers in the supercooled liquid state is mainly driven by the temperature to overcome the kinetics barrier. Differently, the core parameter dominating the fiber drawing process is the viscosity. Figure 1(c) illustrates the range of viscosity required for fiber drawing by rod-in-tube methods.

The temperature dependence of viscosity for glass is fitted to the Mauro–Yue–Ellison–Gupta–Alla model [22]:

$$\log \eta(T) = \log \eta_{\infty} + (12 - \log \eta_{\infty}) \frac{T_g}{T} \times \exp \left[\left(\frac{m}{12 - \log \eta_{\infty}} - 1 \right) \left(\frac{T_g}{T} - 1 \right) \right] \quad (1)$$

where η_{∞} is the high-temperature viscosity limit, which was estimated to be $10^{-2.93}$ Pa·s. m is the melt fragility index,

which describes the change rate of viscosity η during cooling through the glass transition, and is defined by the slope of the logarithmic viscosity near T_g [25–27]:

$$m = \frac{d \log_{10} \eta}{d(T_g/T)_{T_g}}. \quad (2)$$

The temperature dependence viscosity of glass systems with different m values (the Angell plot) is shown in figure S1. Generally, in the glass system with smaller melt fragility, its viscosity exhibits slower average rate of change at the whole supercooled liquid state. Thus, m is a suitable parameter to estimate the viscosity evolution behavior of the glass melt system [28, 29]. Take the commercial fiber materials, such as silica and germanium oxide glass as examples, they have low melt fragility ($m \approx 17$ – 20) (figures 1(d) and S1). In this case, large temperature span (ranging at $1.0 T_g \sim 2.0 T_g$) in the supercooled liquid state is able to reach the suitable viscosity for fiber drawing, leading to better spinnability and wider

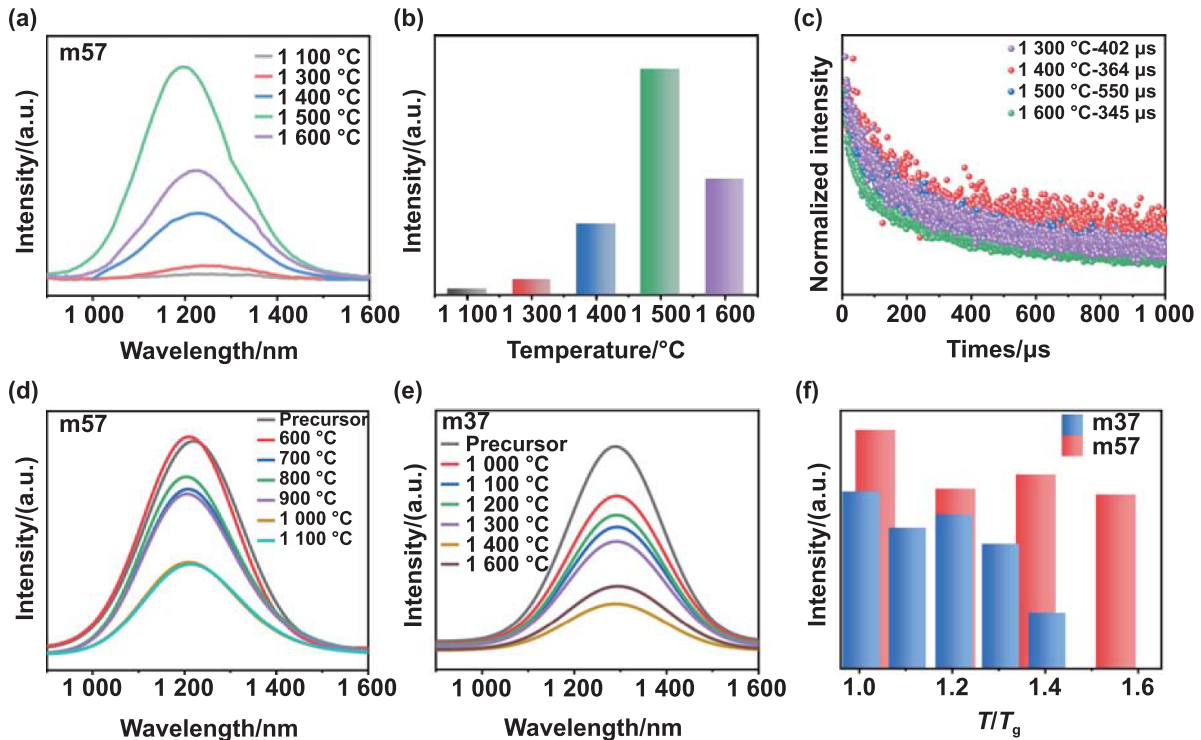


Figure 2. Viscosity evolutionary behavior mediated strategy for improving the stability of optical activity in Bi-doped photonic glass. (a) Emission spectra of Bi-doped m57 glass samples at different melt states. (b) Variation of luminescence intensity with melting temperature for Bi-doped m57 glass samples. (c) Decay curves of Bi-doped m57 glass samples at different melting temperatures. (d) Emission spectra of Bi-doped m57 glass samples at different supercooled liquid states. (e) Emission spectra of Bi-doped m37 glass samples at different supercooled liquid states. (f) Variation of luminescence intensity with the characteristic parameter (T/T_g) for m57 and m37 glass samples.

fiberizing window [25, 26]. However, this may also easily induce the deactivation of the BACs during rod-in-tube fiber drawing process (figure 1(b)). Considering the above fact, by increase the melt fragility, the viscosity of melt will change faster near T_g , which means a reduced temperature span of fiber-drawing. It can be expected that rational tune of the viscosity-temperature dependence may potentially change this situation.

In order to prove the feasibility of the viscosity evolutionary behavior mediated strategy, we focus on the borate glass because it is a typical fragile glass with high melt fragility [28, 29]. As shown in figure 1(d), the viscosity of boron oxide is highly sensitive to the temperature variation with the slope value 1.8 times higher than that of silica and germanate at around T_g . Obviously, reduced temperature span (ranging from $1.0 T_g$ to $1.6 T_g$) in the supercooled liquid state leads to spinnability but it is enough for accomplishing the fiber drawing. More importantly, the characteristic temperature of fiber drawing, which corresponds to the minimum viscosity point and is located in the yellow neck region in figure 1(c), can also be greatly reduced from $2.00 T_g$ for silica and germanate to $1.73 T_g$ for borate oxide. This can be expected to notably relieve the Bi deactivation process in supercooled liquid states.

To verify the feasibility of our strategy, the BACY borate glass with the molar composition of $77B_2O_3-5Al_2O_3-15CaO-3Y_2O_3$ was chosen as the host of Bi for demonstration. The viscosity curve of BACY across the range of

$1.0 T_g \sim 2.0 T_g$ has been obtained and presented in figure 1(d) and the Angell plot is presented in figure S1.

Because of the high melt fragility of BACY ($m = 57$, labeled as m57), a wide range of states with different viscosity ($10^{0.3} \text{ Pa}\cdot\text{s} \sim 10^{7.6} \text{ Pa}\cdot\text{s}$) can be achieved in a limited temperature scope. Firstly, the evolution process of Bi centers in different melt states of m57 was reflected in the NIR emission properties. Figures 2(a) and (b) present the NIR emission spectra of samples achieved from different melt states. They exhibit broadband NIR luminescence at 1220 nm with the full width at half maximum of 230 nm. It can be ascribed to the radiative electronic transitions of BACs. Interestingly, it can be seen that the melting temperature greatly influences the luminescence properties. As the melting temperature increases from 1100 °C to 1500 °C, the NIR emission intensity presents a 35-fold enhancement, which indicates the significant increase in the amount of BAC (Bi^+ , Bi^0 and Bi clusters). The decay dynamics of NIR luminescence was characterized and the results are presented in figure 2(c). The melting temperature dependent decay dynamics followed the similar trend with the emission intensity and the longest decay lifetime was estimated to be 550 μs at 1500 °C. The results demonstrate that the melt state achieved with the high temperature is favorable for driving the dynamic chain reactions from Bi^{3+} to Bi^+/Bi^0 or Bi clusters. A further increase of melting temperature, however, leads to the decrease of the emission intensity. This is mainly associated with the unexpected concentration quenching arising

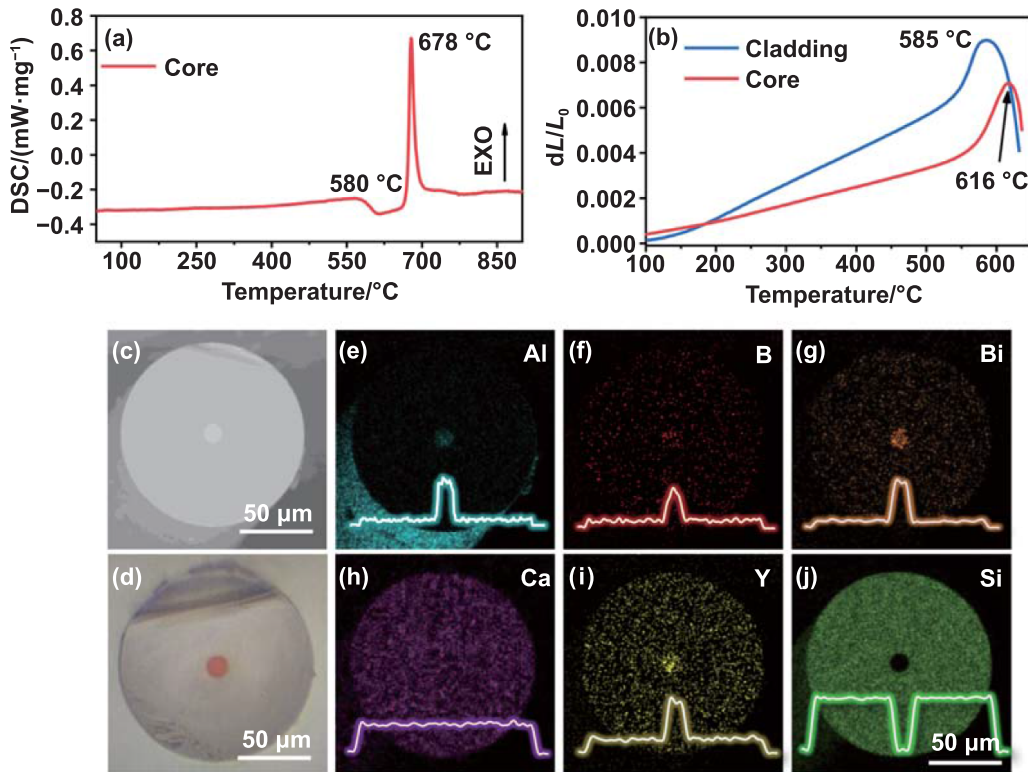


Figure 3. Construction of Bi-doped active m57 fiber. (a) DSC curve of m57. (b) The thermal expansion curves of m57 and K9 glass. (c), (d) SEM photograph (c) and optical micrograph (d) of the fiber's cross-section. (e)–(j) EDS elemental mapping on the fiber's cross-section.

from increasing BAC amount [30]. Eventually, the melting temperature of 1500 °C was chosen for fabrication of the Bi-activated m57 bulk precursor glass rod.

Secondly, the deactivation of the BACs during fiber drawing process in the supercooled liquid state is also estimated. The evolution process of Bi centers in different supercooled liquid states was investigated and can be also indicated by the NIR emission properties. For comparison, a strong SACY silicate glass ($m \approx 37$, labeled as m37) with the molar composition of $77\text{SiO}_2-5\text{Al}_2\text{O}_3-15\text{CaO}-3\text{Y}_2\text{O}_3$ was also investigated. Various supercooled liquid states were achieved by heat-treatment at different temperatures below the melting temperatures. The supercooled liquid states dependent NIR emission spectra of sample m57 and m37 are presented in figures 2(d) and (e). It can be observed that the heat-treatment at the supercooled liquid state leads to the decrease of NIR luminescence intensity. This is consistent with the above statement that BACs are metastable in supercooled liquid states and can easily change into Bi metal particles. Correlation of characteristic parameter (T/T_g) with the integrated NIR emission intensity is summarized and exhibited in figure 2(f). Notably, the changing trend of emission intensity for sample m37 and m57 is totally different in the fiber drawing window ($1.1 T_g \sim 1.6 T_g$). For sample m37, the NIR activity is reduced by a quarter at $1.4 T_g$. The results indicate the strong Bi deactivation during fiber drawing process for sample m37. In detail, because sample m37 is a typical strong glass, large temperature span above T_g is able to reach the suitable viscosity for fiber drawing. In

this process, the metastable BACs easily transfer into inactive Bi metal particles, leading to severe thermal degradation of NIR emission. In contrast, for sample m57, the degradation of luminescence can be well prevented and 82% NIR activity can be maintained at $1.4 T_g$. The results demonstrate that the deactivation of the BACs can be well avoided in sample m57 because of relatively high melt fragility, thus proving the effectivity of viscosity evolutionary behavior mediated strategy.

2.2. Manufacturing of Bi-activated fiber

Inspired by the success in prevention of undesired degradation of optical activity in Bi-doped photonic glass, novel active fiber can be developed. Firstly, the thermal properties of the photonic glass (m57) were studied. The differential scanning calorimetry (DSC) curve of the glass preform is exhibited in figure 3(a), which shows that the characteristic glass transition (T_g) and crystallization (T_c) temperatures are at ~ 580 °C and 678 °C, respectively. In order to guarantee the fiber could be drawn continuously and uniformly, the thermal expansion properties were conducted. The thermal expansion curves of core m57 glass and the selected cladding glass (K9) were compared in figure 3(b). The thermal expansion coefficient of m57 is smaller than that of K9. The softening temperature (T_f) of the former is higher than that of the latter. For fiber drawing, the temperature was set to be ~ 850 °C. Because the refractive indexes of m57 and K9 are 1.602 1 and 1.515 0, respectively, and the designed diameter of the fiber core/cladding is 1:10. As

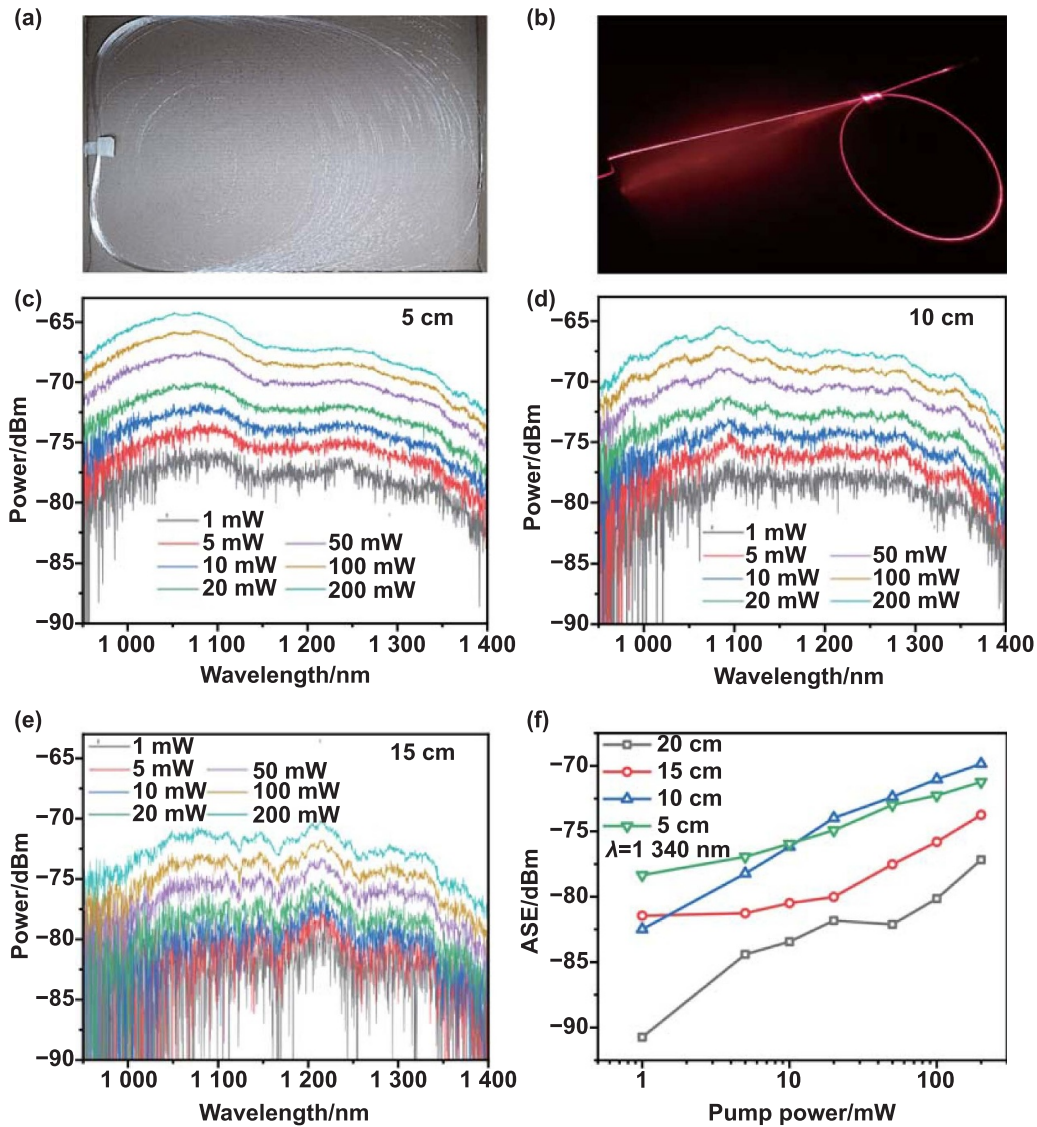


Figure 4. Optical properties of Bi-doped active m57 fiber. (a) Photograph of a bundle of Bi-doped m57 fiber. (b) Photograph of 650 nm laser propagation in 0.5 m long Bi-doped m57 fiber. (c)–(e) ASE spectra (c) 5 cm, (d) 10 cm, (e) 15 cm long Bi-doped fiber under excitation with 808 nm. (f) ASE at 1340 nm versus the length of the Bi-doped fiber under various pump powers.

a result, the multi-mode fiber can be fabricated after thermal drawing.

The scanning electron microscope (SEM) and optical micrograph of the Bi-doped m57 fiber were shown in figures 3(c) and (d). The boundary between fiber core and cladding is clear. The diameter of the fiber core and cladding is estimated to be about 13 μm and 125 μm , respectively. The fiber core shows the same brown color as the preformed Bi-doped m57 photonic glass, which indicates that BACs in core glass are preserved well during fiber drawing. The element distribution analysis of the fiber cross section was performed by the attached energy dispersive spectroscopy (EDS) and the results are shown in figures 3(e)–(j). It can be observed that the elements of Al, B, Ca and Y are homogenous distributed in both core and cladding, and Bi and Si are mainly enriched in the core and cladding, respectively.

The fabricated Bi-doped active m57 fiber exhibits high optical quality. As shown in figure 4(a), rather long (above 100 m) and continuous fiber can be fabricated in 1.5 h. The pumping light can well propagate along the fiber (figure 4(b)). The optical properties of active fiber were studied. The measurement of the loss of the fiber is shown in figure S2. As shown in figure S2(a), to link with the light source, the fibers with different lengths are plugged into the ceramic ferrules to connect to the commercial single mode fiber. With the input power of 30 dBm, the total loss of the fibers with different length are shown in figure S2(b) and the transmission loss of the fiber at 1480 nm is estimated to be 0.024 dB cm^{-1} . Figures 4(c)–(f) exhibit the amplified spontaneous emission (ASE) performance of the active fiber with different length under excitation with 808 nm with different pump power. The ASE spectra are featured by a broad emission band covering the whole

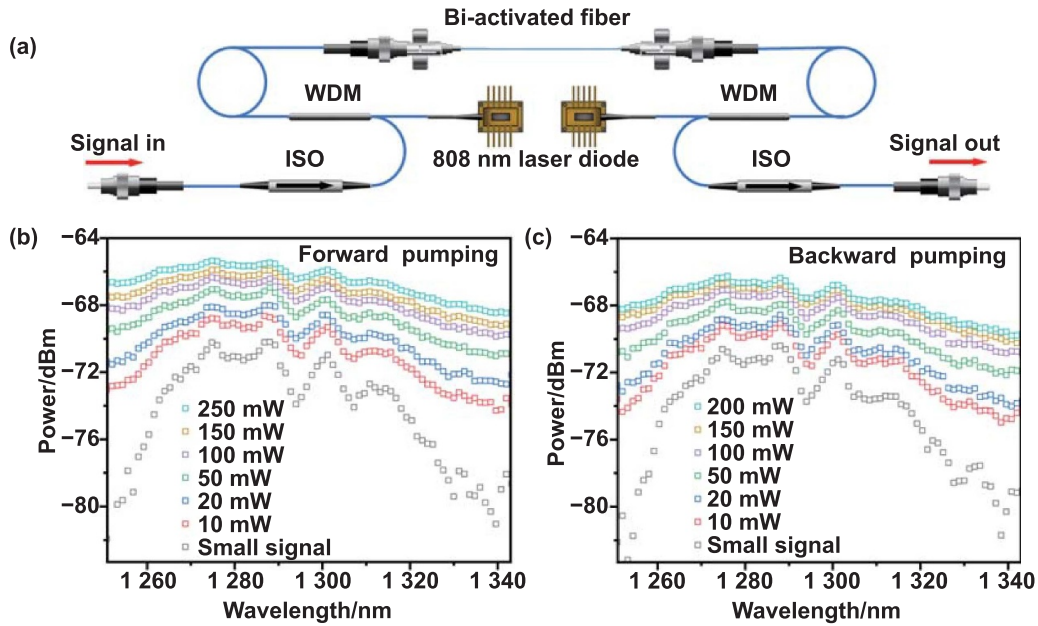


Figure 5. Fiber device based on the Bi-doped active m57 fiber. (a) The schematic drawing illustrates the configuration of the principal Bi-doped fiber amplifier (BDF). (b) The launched small signal and amplified signal spectra by using a 5 cm long Bi-doped fiber under forward pumping scheme. (c) The launched small signal and the amplified signal spectra by using a 5 cm long Bi-doped fiber under backward pumping.

1000 ~ 1400 nm. As the pump power increases, the ASE intensity increases monotonously. With the extension of the fiber length more than 10 cm, the ASE intensity significantly decreases. This is mainly induced by the balance between the emission and transmission losses. In addition, the ASE intensity of the short-wavelength section decreases faster than that at the long-wavelength section. This can be explained from the self-absorption effect which is characterized by the transferring of the high energy photons to the low energy photons [31]. Figure 4(d) depicts a typical relation among the ASE intensity at 1340 nm, the pump power and the fiber length. Furthermore, a 64 dB/5 cm ASE at the pump power of 200 mW (1073 nm) was realized. It is necessary to point out that this is the first time to achieve ASE in Bi-activated borate fiber, which is significant because it is widely recognized that ASE is the basis and premise for developing fiber device [32].

2.3. Optical amplification with the Bi-activated fiber

By using the Bi-doped m57 fiber, we have constructed the fiber amplifier device. The configuration of the principal device is illustrated in figure 5(a). An 808 nm laser diode (LD) was used as pump source and a broadband light source was used as a signal source with the maximum power about -50 dBm. Pump and signal source were coupled by wavelength division multiplexer. The variation of spectra with series pump powers for forward and backward pumping was examined on an optical spectrum analyzer (OSA Yokogawa AQ6370). Isolator (ISO) was used to protect the signal source and spectrum analyzer. In order to easily link with the light source and spectrum analyzer, 5 cm Bi-doped m57 fiber with ceramic ferrules was plugged in by flange and connected with a single-mode

fiber. The optical amplification performance of the device was summarized in figures 5(b) and (c). Without pumping, the power of the signal after passing through the fiber is -70 dBm, which is caused by the coupling loss. The original optical signal in the waveband region of 1250 ~ 1340 nm can be obviously amplified with the pump power increasing from 10 mW to 250 mW. By subtracting the initial signal spectra from the amplified signal spectra, a maximal on-off gain can be achieved by forward pumping scheme with the maximum output of -66 dBm. In the case of backward pumping scheme, the on-off gain can also be observed with the maximum output of -67 dBm. To the best of our knowledge, it is the first time to report optical amplification in Bi-doped borate system, which demonstrates the effectiveness of the proposed viscosity evolutionary behavior mediated strategy, as well as indicates its great potential for application in the high-capacity telecommunication system.

3. Conclusion

In summary, we have proposed and demonstrated a viscosity evolutionary behavior mediated strategy for construction of Bi-doped active fiber with high dopant solubility. The intrinsic mechanism and dependence among the evolution of Bi, reaction temperature and viscosity of the glass system has been elucidated and built. Guided by above relationship, the unexpected overlapping between Bi activation during melting and deactivation during fiber drawing has been avoided. Importantly, for the first time, we have fabricated borate fiber with heavily doped Bi and high optical activity. Furthermore, the principal fiber amplifier device has been constructed and broadband optical signal amplification has

been realized. Our findings demonstrate the effectiveness of the proposed viscosity evolutionary behavior mediated strategy for developing novel photonic active fiber. Apart from that, they indicate its great potential for application in the next-generation high-capacity telecommunication system.

4. Materials and methods

The borate glasses were designed based on the phase diagram of the borate material system. The final composition of the BACY glass was optimized to be $77\text{B}_2\text{O}_3\text{-}5\text{Al}_2\text{O}_3\text{-}15\text{CaO}\text{-}3\text{Y}_2\text{O}_3\text{-}3\text{Bi}_2\text{O}_3$ (mol%, named as m57). The glasses were fabricated by the melting- quenching method. As a typical synthesis procedure, high pure B_2O_3 , Al_2O_3 , CaCO_3 , Y_2O_3 and Bi_2O_3 (99.99 mol%) were used as raw materials. The batches of ~ 30 g for glass composition were weighted and well mixed in an agate mortar and then melted in corundum crucibles at the temperature of 1100°C , 1300°C , 1400°C , 1500°C and 1600°C for 30 min. The melt was subsequently cast onto a brass plate and pressed immediately with another plate. The obtained bulk glass was then cut and finely polished for further characterizations.

For comparison, a silicate glass with composition of $77\text{SiO}_2\text{-}5\text{Al}_2\text{O}_3\text{-}15\text{CaO}\text{-}3\text{Y}_2\text{O}_3\text{-}0.5\text{Bi}_2\text{O}_3$ (mol%, named as m37) was prepared following the same procedure as the control group. Such silicate glass exhibits quite similar optical properties compared to the BACY (m57) bulk glass, such as its emission waveband and intensity, but quite different temperature dependent viscosity behavior (for BACY, $m \approx 57$; for SACY, $m \approx 37$). Thus SACY is selected as control group to investigate the influence of temperature dependent viscosity behavior on the activation of the Bi dopant during different heat history.

The Bi-doped fiber was fabricated with rod-in-tube technology. The core rod of the Bi-doped borate glass fiber was fabricated by the melting and quenching technique with the same composition as m57. A batch of ~ 50 g was weight and mixed. The raw materials poured in a corundum crucible at 1500°C for 30 min. The melt was poured into a graphite mold preheated to 500°C and annealed at 500°C for 6 h. Finally, the annealed glass was cut, lathed and polished to obtained the core rod with the designed dimension. The initial dimension of core rod was 3 mm in diameter and 4 cm in length.

It is hard to fabricate multicomponent bulk glass with similar composition of the rod with large enough scale and high quality as the clad. Thus, we need to choose commercial glass as the clad. K9 glass ($69.13\text{SiO}_2\text{-}10.75\text{B}_2\text{O}_3\text{-}3.07\text{BaO}\text{-}10.40\text{Na}_2\text{O}\text{-}6.29\text{K}_2\text{O}\text{-}0.36\text{As}_2\text{O}_3$, mol%) is one of the most widely used commercial glasses, which is convenient to be obtained the large sized and high quality ones. The K9 glass rod was chosen as the cladding of the fiber perform with an outer diameter of 30 mm and inner diameter of 3 mm. The assembled preform was continuously fabricated into tiny and smooth fiber with a diameter of $\sim 125\ \mu\text{m}$ by thermal drawing process at $\sim 850^\circ\text{C}$. Because the softening point was diverse from the single-mode silica fiber to BDF, ceramic ferrules were used to replace fiber splicing. Two ends of selected

length BDF were inserted and fixed into ceramic ferrules with glue. Then, the end faces were finely polished. Samples of series lengths were prepared for further measurement and characterization.

NIR luminescence spectra under 808 nm LD excitation were recorded through a Zolix Omni $\lambda 3007$ spectrometer equipped with an InGaAs photodetector and an SR830 Stanford Research lock-in amplifier. Luminescence lifetime was taken using an Edinburgh FLS920 spectrofluorometer equipped with a liquid nitrogen-cooled photomultiplier (Hamamatsu R5509-72). A 450 W xenon lamp and a micro-second flashlamp (μF900) were used as the excitation sources. The thermal properties of glass were measured by DSC using an STA449C Jupiter (Netzsch, Bavaria, Germany) instrument at a heating rate of $10\ \text{K}\ \text{min}^{-1}$. The thermal expansion properties were characterized by thermodilatometry (DIL 402 C/41G). The refractive index was measured by prism coupling (model 2010) after the surface of glass sample was fine polished. The cross-section structure and the element distribution were investigated by SEM (ZEISS EVO18) and the attached EDS.

Acknowledgments

The authors gratefully acknowledge financial support from the National Key R&D Program of China (2020YFB1805901), the National Science Fund for Distinguished Young Scholars (62125502), the National Natural Science Foundation of China (51972113, 52302002 and 62305115), the Local Innovative and Research Teams Project of Guangdong Pearl River Talents Program (2017BT01X137), Foshan Science and Technology Innovation Project (1920001000052), the Foundation of State Key Laboratory of Reactor System Design Technology, the Large Scientific Facility Open Subject of Songshan Lake, Dongguan, Guangdong, the Research Project supported by State Key Lab of Luminescent Materials and Devices, South China University of Technology (Skllmd-2023-07) and the Sponsored Research Project of Corning Incorporated.

ORCID iDs

Jianrong Qiu  <https://orcid.org/0000-0003-3148-2500>
Shifeng Zhou  <https://orcid.org/0000-0003-4609-763X>

References

- [1] Temprana E, Myslivets E, Kuo B P P, Liu L, Ataie V, Alic N and Radic S 2015 Overcoming Kerr-induced capacity limit in optical fiber transmission *Science* **348** 1445–8
- [2] Rapp L and Eiselt M 2022 Optical amplifiers for multi-band optical transmission systems *J. Lightwave Technol.* **40** 1579–89
- [3] Dianov E M 2013 Amplification in extended transmission bands using bismuth-doped optical fibers *J. Lightwave Technol.* **31** 681–8
- [4] Thipparapu N K, Wang Y, Wang S, Umnikov A A, Barua P and Sahu J K 2019 Bi-doped fiber amplifiers and lasers *Opt. Mater. Express* **9** 2446–65

- [5] Dvoyrin V V, Mashinsky V M, Dianov E M, Umnikov A A, Yashkov M V and Guryanov A N 2005 Absorption, fluorescence and optical amplification in MCVD bismuth-doped silica glass optical fibres *31st European Conf. on Optical Communication (Glasgow, UK)* (IEEE) pp 949–50
- [6] Vakhrushev A S et al 2022 W-type and Graded-index bismuth-doped fibers for efficient lasers and amplifiers operating in E-band *Opt. Express* **30** 1490–8
- [7] Optical Fiber Cable and Connectivity Solutions (OFS) 2023 Optical amplification *optical amplifiers* (available at: www.ofsoptics.com/amplification/)
- [8] Bufetov I A and Dianov E M 2009 Bi-doped fiber lasers *Laser Phys. Lett.* **6** 487–504
- [9] Ruan J, Wu E, Zeng H P, Zhou S F, Lakshminarayana G and Qiu J R 2008 Enhanced broadband near-infrared luminescence and optical amplification in Yb–Bi codoped phosphate glasses *Appl. Phys. Lett.* **92** 101121
- [10] Peng M Y, Dong G P, Wondraczek L, Zhang L L, Zhang N and Qiu J R 2011 Discussion on the origin of NIR emission from Bi-doped materials *J. Non-Cryst. Solids* **357** 2241–5
- [11] Cao J K, Li L Y, Wang L P, Li X M, Zhang Z Y, Xu S H and Peng M Y 2018 Creating and stabilizing Bi NIR-emitting centers in low Bi content materials by topo-chemical reduction and tailoring of the local glass structure *J. Mater. Chem. C* **6** 5384–90
- [12] Sidebottom D L, Tran T D and Schnell S E 2014 Building up a weaker network: the effect of intermediate range glass structure on liquid fragility *J. Non-Cryst. Solids* **402** 16–20
- [13] Zachariasen W H 1932 The atomic arrangement in glass *J. Am. Chem. Soc.* **54** 3841–51
- [14] Khagai A M, Alyshev S V, Vakhrushev A S, Riumkin K E, Umnikov A A and Firstov S V 2022 Recent advances in Bi-doped silica-based optical fibers: a short review *J. Non-Cryst. Solids X* **16** 100126
- [15] Wallenberger F T and Bingham P A 2010 *Fiberglass and Glass Technology: Energy-friendly Compositions and Applications* (Springer)
- [16] Tian J M, Guo M T, Wang F, Wu C, Zhang L, Wang M, Wang Y F, Chen J, Yu C L and Hu L L 2023 High gain optical amplification and lasing performance of the Bi/P co-doped silica fiber in the O-band *Chin. Opt. Lett.* **21** 050601
- [17] Chang J, Wang Q P, Zhang X Y, Liu Z J, Liu Z J and Peng G D 2006 S+C band optical amplification in Er³⁺-Tm³⁺ co-doped fiber *Chin. Opt. Lett.* **4** 66–68
- [18] Sidebottom D L 2019 Connecting glass-forming fragility to network topology *Front. Mater.* **6** 144
- [19] Tao G M, Ebendorff-Heidepriem H, Stolyarov A M, Danto S, Badding J V, Fink Y, Ballato J and Abouraddy A F 2015 Infrared fibers *Adv. Opt. Photonics* **7** 379–458
- [20] Zou Y Q, Liu C, Ren Z H, Zhang Y Q, Liu Z C, Xu Y S, Hou C, Yang L, Liang S and Tao G M 2022 Flexible and robust low-loss selenium-based multimaterial infrared fibers towards CO₂ laser ablation *iScience* **25** 105167
- [21] Tao G M, Stolyarov A M and Abouraddy A F 2012 Multimaterial fibers *Int. J. Appl. Glass Sci.* **3** 349–68
- [22] Mauro J C, Yue Y Z, Ellison A J, Gupta P K and Allan D C 2009 Viscosity of glass-forming liquids *Proc. Natl Acad. Sci. USA* **106** 19780–4
- [23] Zheng Q J, Mauro J C and Yue Y Z 2017 Reconciling calorimetric and kinetic fragilities of glass-forming liquids *J. Non-Cryst. Solids* **456** 95–100
- [24] Yue Y Z, Von Der Ohe R and Jensen S L 2004 Fictive temperature, cooling rate, and viscosity of glasses *J. Chem. Phys.* **120** 8053–9
- [25] Angell C A 1995 Formation of glasses from liquids and biopolymers *Science* **267** 1924–35
- [26] Angell C A 1988 Structural instability and relaxation in liquid and glassy phases near the fragile liquid limit *J. Non-Cryst. Solids* **102** 205–21
- [27] Debenedetti P G and Stillinger F H 2001 Supercooled liquids and the glass transition *Nature* **410** 259–67
- [28] Page A G, Bechert M, Gallaire F and Sorin F 2019 Unraveling radial dependency effects in fiber thermal drawing *Appl. Phys. Lett.* **115** 044102
- [29] Yue Y Z and Zheng Q J 2017 Fiber spinnability of glass melts *Int. J. Appl. Glass Sci.* **8** 37–47
- [30] Peng M Y, Zollfrank C and Wondraczek L 2009 Origin of broad NIR photoluminescence in bismuthate glass and Bi-doped glasses at room temperature *J. Phys.: Condens. Matter* **21** 285106
- [31] Wang D C, Pei L, Zheng J J, Wang J S, Xu W X, Ning T G, Li J and Wang L H 2022 Analysis of gain and noise characteristics of O-band Bi-doped fiber amplifier under different pumping schemes *Optik* **251** 168491
- [32] Lai F S, Jou J J and Liu C K 1999 Indicator of amplified spontaneous emission in erbium-doped fibre amplifiers *Electron. Lett.* **35** 587–8